First 0ν results from EXO–200 experiment

D.J. Auty on behalf of the EXO Collaboration
Department of Physics and Astronomy, University of Alabama,206 Gallalee Hall, Tuscaloosa, AL 35487, United States of America

EXO–200 is a double-beta decay experiment that measures the half-life of the decay of ^{136}Xe. This article describes the result reported by EXO–200 in the summer 2012, which saw no signal for the 0 $\nu\beta\beta$ decay which used an exposure of 32.5 kg·yr. This sets a lower limit for the half-life of the neutrinoless double-beta decay $\mathrm{T}^{0\nu\beta\beta}_{1/2}$ (^{136}Xe)> 1.6×10^{25}yr(90 % CL), which sets a limit on the Majorana neutrino mass, depending on which matrix element used, of 140 meV–380 meV.

1 Introduction

The Standard Model of particle physics (SM) has been experimentally tested to extremely high precision. The first direct evidence that the SM is incomplete has come with the discovery that neutrinos are massive. The study of neutrino properties, therefore, directly probes new physics beyond the SM.

In the SM, double beta-decay is a second order weak interaction that some even-even nuclides undergo, where single beta decay is energetically forbidden or highly spin suppressed due to large angular momentum differences. In the SM this decay can happen through two neutrino double beta decay ($2\nu\beta\beta$), which has been observed in a handful of nuclides and typically has a half-life of $\sim10^{20}$yr. The half-life for $2\nu\beta\beta$ is only related to the phase space ($G^{2\nu}$)and nuclear matrix element ($M^{2\nu}$)

$$ {}^{2\nu\beta\beta}_{1/2}T^{-1} = G^{2\nu} \cdot \left|M^{2\nu}\right|^2 , \tag{1}$$

and unrelated to the properties of the neutrino. If neutrinos are unlike the charged fermions, which are Dirac particles [1], and are Majorana particles [2], then the double beta decay could happen without the emission of neutrinos ($0\nu\beta\beta$), which would violate conservation of B-L. The rate of this process is given by

$$ {}^{0\nu\beta\beta}_{1/2}T^{-1} = G^{0\nu} \cdot \left|M^{0\nu}\right|^2 \cdot \langle m_{\beta\beta}\rangle \tag{2}$$

where $G^{0\nu}$ is a phase space and $M^{0\nu}$ is the nuclear matrix element and $m_{\beta\beta}$ is the Majorana neutrino mass. So the rate of $0\nu\beta\beta$ is dependent of the Majorana neutrino mass. These two processes have very different energy spectra for the electrons emitted. In the two neutrino case the summed energy of the two electrons have a continuous spectrum with the endpoint at the Q-value, while the zero neutrino case the summed energy is peaked at the Q-value.

A handful of isotopes have already been seen to undergo $2\nu\beta\beta$ decay. One controversial claimed observation of $0\nu\beta\beta$, with ^{76}Ge, has been made [4]. Using different isotopes to the claimed observation, can help define the neutrino mass through refining the matrix elements. Also using different isotopes help verify the claim, as they have different Q-values, so they

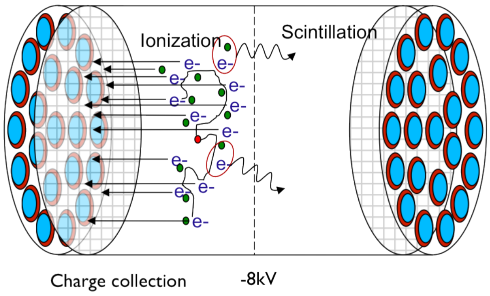

Figure 1: Cartoon of the EXO–200 TPC with the Cathode in the centre plan and the charge collection wires and APD's at either end.

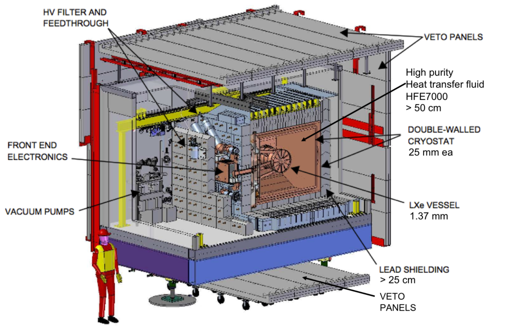

Figure 2: Cutaway view of the EXO-200 setup, with the primary subassemblies identified.

exclude the possibility that the signal was an unknown background. One of the isotopes of interest for $0\nu\beta\beta$ search is ^{136}Xe, which has a high Q-value (2457.83 ± 0.37 keV[3]) so is above most natural radiation. Isotropic enrichment is also relatively easy in comparison with other candidate isotopes as it is the heaviest long-lived isotope of xenon. It is a nobel gas so can be easily cleaned continuously and has a low rate of $2\nu\beta\beta$ decay which was first observed with EXO-200[5] $2.11\pm0.04(\mathrm{stat})\pm0.21(\mathrm{syst})\times10^{21}$ yr. It also has the potential to tag the daughter ion ^{136}Ba thus making the measurement background free.

2 EXO–200

EXO–200 is the prototype detector for the EXO collaboration and is located at the Waste Isolation Pilot Plant (WIPP) in New Mexico, USA. The main focus of EXO–200 was to achieve good energy resolution at the Q-value of ^{136}Xe and also to have low backgrounds. This was achieved by taking advantage of event topology. EXO–200 uses xenon as both the $\beta\beta$ source and the detector of the summed electron energy. It uses 200 kg, of which 175 kg is in liquid phase, of xenon enriched to (80.6 ± 0.1) % in the isotope ^{136}Xe. The remaining 19.4 % is ^{134}Xe, with other isotopes present only at low concentration. At operating temperature, 167 K, and a pressure, 147 kPa, the liquid xenon (LXe) has a density of 3.0 g cm^{-3}. The LXe is contained within a thin wall cylindrical copper time projection chamber (TPC) with a cathode grid held at -8 kV at the mid plane, splitting the TPC into two (figure 1). Charge is collected at each end of the TPC on wire plains ("U" wires) that are held at a virtual ground, while the 178 nm-wavelength scintillation light is collected on two arrays of large area avalanche photodiodes (LAAPDs), which are located behind the collection planes. A second wire plane ("V" wires) in front of the charge collection plane, and rotated 60° from it, is biased so that it is fully transparent to electrons and is used to inductively record a second co-ordinate channel. To get full three demential reconstruction, the z-position is calculated by the difference in arrival time between the scintillation signal and the charge signal.

The event topography in the TPC allows rejection of alpha and cosmic muons from $\beta\beta$ like events. γ-rays produced from nuclear decays are likely to interact in multiple sites within the TPC (MS) so can be tagged, whilst $\beta\beta$ events are point-like energy dispositions (SS). This is not 100 % efficient at separating events, so the active Xe region needs to be intrinsically clean. This was achieved by cleaning all the components and measuring their radioactivity. So the TPC was made from the most radiopure substances[6]. The TPC is encased in at least 50 cm of high purity HFE-7000[7], which keeps the TPC in thermal contact with the inner cryostat wall, and 25 cm of lead to further reduce external radioactivity. EXO–200 is situated $\sim$1600 mwe underground, thus reducing the cosmic muon rate to a flux of 1.5×10^{5} yr^{-1} m^{-2} sr^{-1} [8], which although low the cosmic-ray muons rate needed to be reduced by a further 90 % if EXO-200 was to meet its goals. To do this 29, $5\times65\times(315|375)$ cm, plastic scintillator panels are installed around the

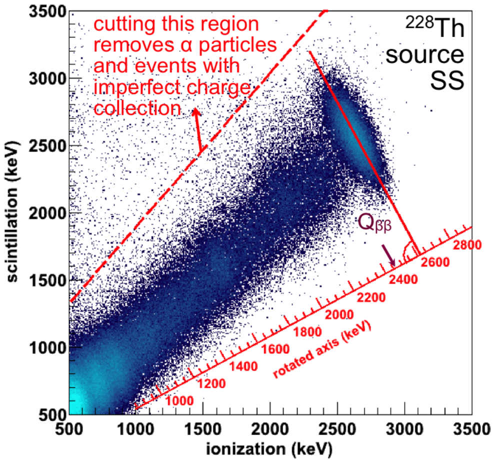

Figure 3: Correlation between ionisation and scintillation for SS events from a 228Th source. The energy resolution is considerably improved by forming the linear combination of both measurements. Events in the top-left quadrant are due to in- complete charge collection and are rejected by the cut (dashed line), removing only 0.5 % of the total. The cut is defined using the gamma ray full absorption islands from three calibration sources.

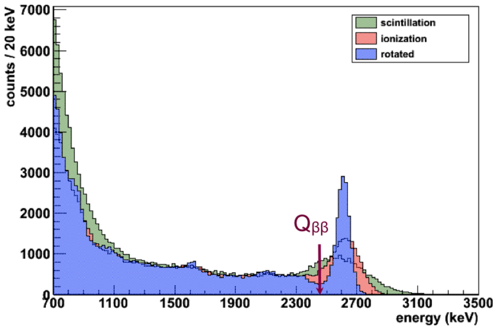

Figure 4: The SS energy spectrum for scintillation only, charge only and rotate energy. It can be seen that the resolution of the 2615 keV peak is reduced from 6.8 % for scintillation and 3.4 % for charge to 1.6 % in the rotated spectrum.

cleanroom to tag muons as they pass through. A drawing of the layout is shown in figure 2. A more in-depth description of the EXO–200 detector and its manufacture is given in [9].

3 Data

The active volume of the LXe for this analysis was the inner 98.5 kg LXe, 79.4 kg of ^{136}Xe. The data analysed was taken between 22nd September 2011 and 16th April 2012, for a total of 2896.6 live hours after cuts [10], which is 32.5 kg·yr livetime. Only events above 700 keV are included in this analysis, as this is where the trigger is 100 % efficient. Other analysis cuts that were used were: events in the TPC that happened 1 μs before or 25 ms after a veto panel triggered were rejected, making the veto efficiency $96.2^{+0.4}_{-3.7}$ % at rejecting cosmic muons (0.58 % dead time); TPC events that happened within one second of each other to be rejected (3.3 % dead time), TPC events that happened within one minute after a muon was reconstructed in the TPC (5.0 % dead time), to reduce the daughter decays following the muon; alpha decays were excluded from the data by the diagonal cut shown if figure 3 as alpha decays have a higher light to charge ratio than beta decays. The total dead time due to the veto cuts was 8.6 %. The stability of the detector was achieved through daily calibrations mostly using the ^{228}Th source (2615 keV), ^{60}Co (1173 keV and 1332 keV) and ^{137}Cs (662 keV) were used less often to calibrate the energy for the full spectrum. The energy from an event can go into light and charge by various amounts, so smearing any peak out in either spectrum. To counter this effect the 2615 keV peak from ^{208}Tl decay was used to “rotate” the light and charge from the known energy of the Tl peak to was used to fix the energy of the rotated spectrum to the true energy (figure 3), and improve the energy resolution compared to scintillation or charge only (figure 4). The residual at each calibration energy of the rotated spectrum, defined as $(E_{fit} - E_{true})/E_{true}$ and the uncertainty bands are shown in top plot in figure 5 and the energy resolution parameterised as $\sigma^2 = a\sigma_e^2 + bE + E^2$ is shown in the bottom plot of figure 5, where σ_e^2 is the electronic noise contribution, bE is the statistical fluctuation in the ionisation and scintillation and cE^2 is the position and time dependant broadening. In the rotated energy spectrum at the Q-value the energy resolution was 1.67 % (1.84 %) SS (MS).

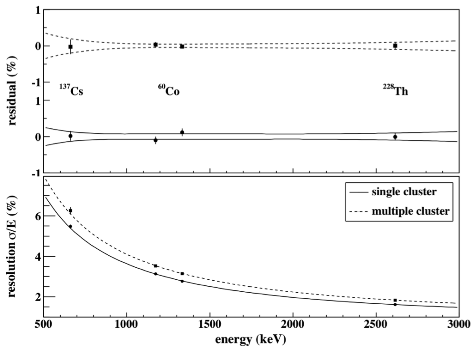

Figure 5: Top: systematic uncertainty bands on the energy calibration residuals, using the full energy reconstruction de- scribed for the three γ sources. For both SS (solid) and MS (dashed) the position of the four γ lines is consistent with the calibration model within $\leq 0.1\,\%$. Bottom: energy resolution for various sources along with a fit to the empirical model discussed in the text. The resolution at the $0\nu\beta\beta$ Q-value is 1.67 % (1.84 %) for SS (MS) events.

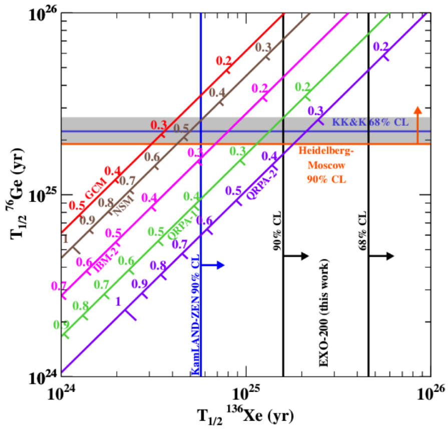

Figure 6: Relation between the $T_{1/2}^{0\nu\beta\beta}$ in ^{76}Ge and ^{136}Xe for different matrix element calculations (GCM [12], NSM [13], IBM-2 [14], RQRPA-1 [15] and QRPA-2 [16]). For each matrix element $\langle m\rangle_{\beta\beta}$ is also shown (eV). The claim [4] is represented by the grey band, along with the best limit for ^{76}Ge [17]. The result reported here is shown along with that from [11].

4 Analysis

The detectors ability to identify SS and MS events to distinguish between SS $\beta/\beta\beta$ events and MS γ events in the bulk xenon. The clustering resolution in two dimensions, U-dimention is 18 cm and 6 mm in z (drift time). The ability of the GEANT4 Monte Carlo (MC) to simulate the distributions for SS and MS energy spectra was proven on the ^{228}Th and ^{60}Co source data (figure 7 for ^{228}Th). The MC reproduces the fraction of SS events, defined as $N_{ss}/(N_{ss}+N_{ms})$ to $\pm\,8.5\,\%$. The requirement that events be fully reconstructed[a] gives an efficiency of 70 % (71 %) for the ^{228}Th ($0\nu\beta\beta$) spectrum. The 71 % efficiency was further verified by comparing the $2\nu\beta\beta$ data spectrum with MC.

Background models were generated for the various components of the detector from the material screening campaign, providing normalisation for the MC generated probability distribution functions (pdfs). These background contributions were estimated using previous generation of detector simulations [9], which account for 50 (0.2) events in the $2\nu\beta\beta$ ($0\nu\beta\beta$) spectrum, were not included in the fit. The various generated pdfs were fitted to the data using a maximum likelihood fit and varied so that SS site events were constrained to be $\pm 8.5\,\%$ of the value predicted by the MC (figure 7). As γ-rays were used to calibrate the detector, the energy of the β events was a free parameter in the fit, so it is constrained by the $2\nu\beta\beta$ events. The fit reports a scale factor of 0.995 $\pm$0.004. The fit gives a expected background of $(1.5{\pm}0.1){\times}10^{-3}\,\mathrm{kg}^{-1}\,\mathrm{yr}^{-1}\,\mathrm{keV}^{-1}$ in the one sigma region of interest (ROI), where one sigma is 1.67 % of 2458 keV(41 keV), which is 3–4 events. Figure 8 shows that there is only one event in this region. It is expected, with this exposure, for one of fewer events to be seen 7 % of the time. In figure 7 it can be seen that there are events greater than 3000 keV in the SS spectrum, these fit to ^{137}Xe. As these events are also where there is a peak in the MS spectrum it was decided to exclude ^{137}Xe from this fit as this gives a more conservative limit on $T_{1/2}^{0\beta\beta}$ and in the next analysis it will be more obvious if these events are leaked MS events or genuine SS events from ^{137}Xe. Also between 2400 keV and 2550 keV for 7 bins the data are above the prediction from the models. However, each point is within one sigma and there is no candidate background that has not been included in the fit. The result from the fit is a $T_{1/2}^{0\beta\beta} > 1.6{\times}10^{25}$ yr with the $T_{1/2}^{2\beta\beta}$ = 2.23$\pm$0.02 (stat.)$\pm$0.22

[a]have charge and scintillation signal

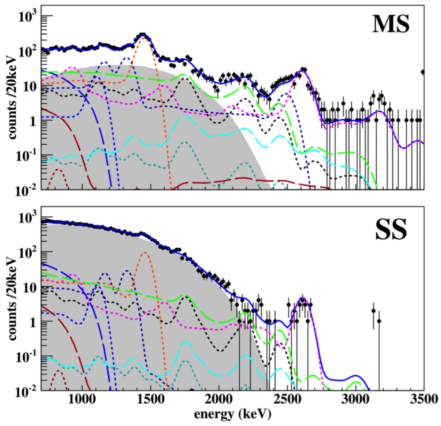

Figure 7: MS (top) and SS (bottom) energy spectra from the 2,896.6 hours of low background data used for this analysis. The best fit line (solid blue) is shown. The background components are $2\nu\beta\beta$ (grey region), ^{40}K (dotted orange), ^{60}Co (dotted dark blue), ^{222}Rn in the cryostat-lead air-gap (long- dashed green), ^{238}U in the TPC vessel (dotted black), ^{232}Th in the TPC vessel (dotted magenta), ^{214}Bi on the cathode (long-dashed cyan), ^{222}Rn outside of the field cage (dotted dark cyan), ^{222}Rn in active xenon (long-dashed brown), ^{135}Xe (long-dashed blue) and ^{54}Mn (dotted brown). The last bin on the right includes overflows. There are no overflows in the SS spectrum.

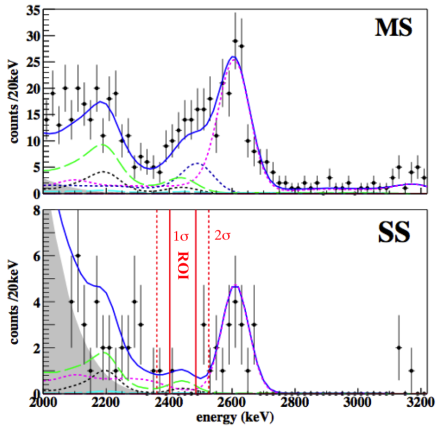

Figure 8: Energy spectra in the ^{136}Xe $Q_{\beta\beta}$ region for MS (top) and SS (bottom) events. The 1 (2)σ regions around $Q_{\beta\beta}$ are shown by solid (dashed) vertical lines. The $0\nu\beta\beta$ PDF from the fit is not visible. The fit results have the same meaning as in figure 7

(syst.)$\times 10^{21}$yr. The dominate systematic errors are from the fiducial volume (12.34 %) and the β scale (9.32 %). $T^{0\beta\beta}_{1/2}$ can be converted into a limit on neutrino mass using various matrix elements which give a neutrino mass between 140 meV and 380 meV at 90 % CL. In Figure 6 the comparison between $T^{0\beta\beta}_{1/2}$ for ^{76}Ge and ^{136}Xe is shown with the predicted Majorana mass of the neutrino, also plotted are the limits set by this analysis and a previous analysis for KamLAND-Zen [11] for ^{136}Xe and the claimed observation and the 90 % limit for ^{76}Ge. It can be seen that for most matrix elements the 90 % limit from EXO is incompatible with the Ge observation.

5 Future

EXO–200 is going to run for five years which will investigate the degenerate region of the mass scale. A tonne scale version is in the planning stage at the moment and if it is just a scaled up version of EXO–200 with the planned upgrades most of the inverse hierarchy can be ruled out, depending on the matrix element used. If Ba tagging is implemented nEXO would investigate the whole inverse hierarchy sector (figure 9) with all matrix elements.

6 Summary

EXO–200 is fully operational now and taken good low background data. It was the first to measure the half-life of the $2\nu\beta\beta$ decay in ^{136}Xe, which is significantly lower than the previous limits set by Bernabei et al [18] and Gavriljuk et al [19]. This equates to a ^{136}Xe $2\nu\beta\beta$ nuclear matrix element of 0.019MeV^{-1}, which is the smallest matrix element directly measured. This result has been confirmed by the KamLAND-Zen [11] collaboration and the second EXO–200 paper [10].

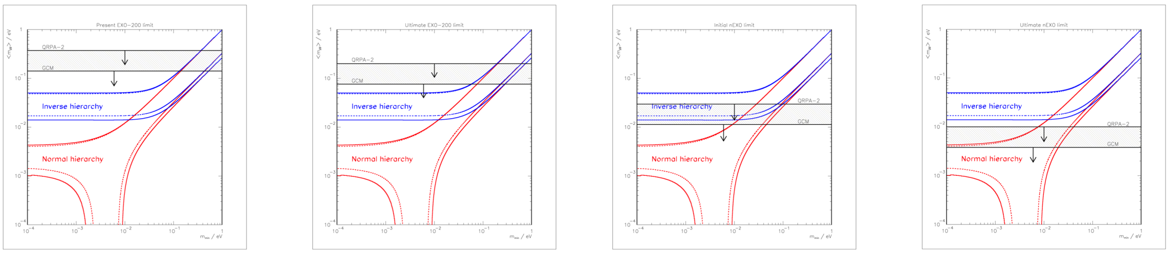

Figure 9: The Majorana mass sensitivities of EXO–200 and nEXO using two likely matrix elements. Left most is this results Majorana mass limits. Next left is the final sensitivity of EXO–200. Right middle is the sensitivity of a 5 tonne nEXO without Ba tagging. Right most is the sensitivity of a 5 tonne nEXO with Ba tagging.

In the second EXO–200 paper a limit on the $0\nu\beta\beta$ half-life that is intension with the claimed measurement from ^{76}Ge, depending on which matrix element is used. With background counts at $(1.5\pm0.1)\times10^{-3}\,\mathrm{kg}^{-1}\,\mathrm{yr}^{-1}\,\mathrm{keV}^{-1}$ and an energy resolution of 1.67 % EXO–200 is working at the design goals of the experiment and measure a Majorana neutrino mass down to below 100 meV. The EXO collaboration is now designing the next phase of the EXO experiment at tonne scale. With this detector and it Ba tagging works nEXO will be able to cover the whole of the inverse hierarchy mass range.

Acknowledgements

EXO–200 is supported by DoE and NSF in the United States, NSERC in Canada, SNF in Switzerland and RFBR in Russa. The collaboration gratefully acknowledges the WIPP for their hospitality

References

1. For instance J. Bjorken and S. Drell *Relativistic Quantum Fields* (McGraw Hill, New York 1965).
2. E. Majorana *Nuovo Cimento* **14**, 171 (1935).
3. M. Redshaw *et al.*, *Phys. Rev. Lett.* **98**, 053003 (2007).
4. H.V. Klapdor-Kleingrothaus and I.V. Krivosheina, *Mod. Phys. Lett.* A **21**, 1547 (2006).
5. N. Ackerman *et al.*, *Phys. Rev. Lett.* **107**, 212501 (2011).
6. D.S. Leonard *et al.*, *Nucl. Instrum. Methods* A **591**, 490 (2008).
7. 3M HFE-7000, http://www.3m.com/.
8. E.I. Esch *et al.*, *Nucl. Instrum. Methods* A **538**, 516 (2005).
9. M. Auger *et al.*, *JINST* **7**, P05010 (2012).
10. M. Auger *et al.*, *Phys. Rev. Lett.* **109**, 032505 (2012).
11. A. Gando *et al.*, *Phys. Rev.* C **85**, 045504 (2012).
12. T.R. Rodriguez and G. Martinez-Pinedo, *Phys. Rev. Lett.* **105**, 252503 (2010).
13. J. Menendez *et al.*, *Nucl. Phys.* A **818**, 139 (2009).
14. J. Barea and F. Iachello, *Phys. Rev.* C **79**, 044301 (2009).
15. F. Simkovic *et al.*, *Phys. Rev.* C **79**, 055501 (2009).
16. A. Staudt, K. Muto and H. V. Klapdor-Kleingrothaus, *Europhys. Lett* **13**, 31 (1990).
17. H.V. Klapdor-Kleingrothaus *et al.*, *Eur Phys. J* A **12**, 147 (2001).
18. R. Bernabei *et al.*, *Phys. Lett.* B **546**, 23 (2002).
19. J. M. Gavriljuk *et al.*, *Phys. Atom. Nucl.* **69**, 2129 (2006).